Supplement of Atmos. Chem. Phys., 18, 12969–12989, 2018
https://doi.org/10.5194/acp-18-12969-2018-supplement

Atmospheric Chemistry and Physics
Open Access
EGU

Supplement of

Gas-to-particle partitioning of major biogenic oxidation products: a study on freshly formed and aged biogenic SOA

Georgios I. Gkatzelis et al.

Correspondence to: Thorsten Hohaus (t.hohaus@fz-juelich.de)

Table S1: Major compounds identified as parent ions from the PTR-based techniques that have been observed in previous publications. Suggested names and structures are attributed to the chemical formula that was identified by the PTR-based techniques.

	Chemical formula	MW	Structure	SMILES code
β-pinene (Hohaus et al., 2015;Chen and Griffin, 2005;Jenkin, 2004;Yu et al., 1999)				
Nopinone	$C_9H_{14}O$	138.21	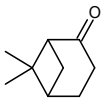	CC1(C2CC1C(=O)CC2)C
2,2-Dimethyl-cyclobutane-1,3-dicarboxaldehyde	$C_8H_{12}O_2$	140.18	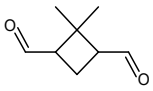	O=CC1CC(C=O)C1(C)C
Oxonopinone	$C_9H_{12}O_2$	152.19	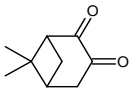	CC1(C2CC1C(=O)C(=O)C2)C
2,2-Dimethyl-3-formyl-cyclobutyl-methanoic acid	$C_8H_{12}O_3$	156.18	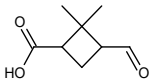	OC(=O)C1CC(C=O)C1(C)C
Norpinonic acid top/ Pinalic-3-acid middle/ Pinalic-4-acid bottom	$C_9H_{14}O_3$	170.21	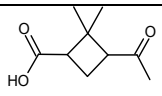	OC(=O)C1CC(C(C)=O)C1(C)C
			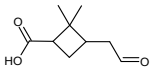	OC(=O)C1CC(CC=O)C1(C)C
			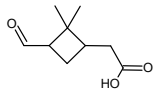	OC(=O)CC1CC(C=O)C1(C)C
Norpinic acid	$C_8H_{12}O_4$	172.18	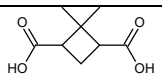	CC1(C(CC1C(=O)O)C(=O)O)C
Hydroxy norpinonic acids	$C_9H_{14}O_4$	186.21	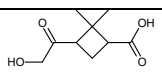	OC(=O)C1CC(C(=O)CO)C1(C)C
			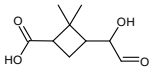	OC(C=O)C1CC(C(=O)O)C1(C)C
Pinic acid	$C_9H_{14}O_4$	186.21	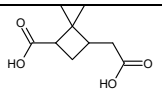	CC1(C(CC1C(=O)O)CC(=O)O)C

Limonene **(Kundu et al., 2012;Jaoui et al., 2006;Chen and Griffin, 2005;Leungsakul et al., 2005b;Leungsakul et al., 2005a)**				
3,6-Oxoheptanoic acid	$C_7H_{10}O_4$	158.15	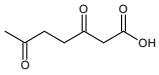	O=C(CCC(C)=O)CC(=O)O
Limonalic acid/ Norlimononic acid/ Ketolimononaldehyde	$C_9H_{14}O_3$	170.21	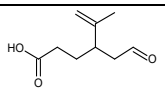	O=CCC(CCC(=O)O)C(=C)C
			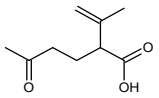	O=C(C)CCC(C(=C)C)C(=O)O
			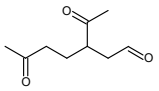	CC(=O)C(CC=O)CCC(=O)C
Limononic acid/ 4-Isopropenyl-1-methyl-1,5-hydroxy-2-oxocyclohexane/ 7-Hydroxylimononaldehyde	$C_{10}H_{16}O_3$	184.23	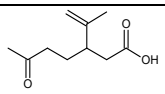	O=C(C)CCC(CC(=O)O)C(=C)C
			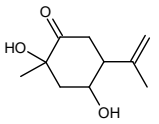	CC(=C)C1CC(=O)C(C)(O)CC1O
			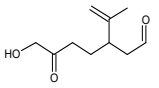	O=C(CCC(CC=O)C(=C)C)CO
Ketolimononic acid/ Limonic acid	$C_9H_{14}O_4$	186.21	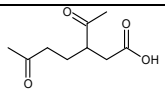	O=C(C)CCC(CC(=O)O)C(C)=O
			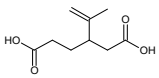	OC(=O)CCC(CC(=O)O)C(=C)C
5-Hydroxylimononic acid/ 7-Hydroxylimononic acid	$C_{10}H_{16}O_4$	200.23	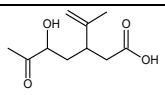	O=C(C)C(O)CC(CC(O)=O)C(=C)C
			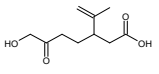	O=C(CCC(CC(=O)O)C(=C)C)CO
Trees (α-pinene / Δ^3-carene) **(Praplan et al., 2014;Chen and Griffin, 2005;Yu et al., 1999)**				
3-Norcaronic acid and isomers	$C_9H_{14}O_3$	170.21		O=C(C)CC1C(C(=O)O)C1(C)C

			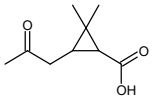	OC(=O)CC1C(CC=O)C1(C)C
			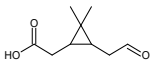	OC(=O)CC1C(CC=O)C1(C)C
			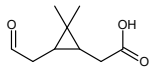	
Norpinic acid / Nor-3-caric acid	$C_8H_{12}O_4$	172.18		CC1(C(CC1C(=O)O)C(=O)O)C
			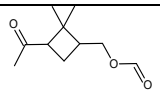	O=C(C)C1CC(COC=O)C1(C)C
2,2-Dimethyl-3-formyl-cyclobutyl-methanoic-acid/ Pinonic acid / 3-caronic acid/ Hydroxy pinonaldehydes	$C_{10}H_{16}O_3$	184.23	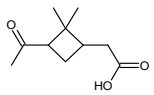	OC(=O)CC1CC(C(C)=O)C1(C)C
			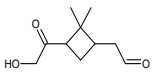	O=C(CO)C1CC(CC=O)C1(C)C
			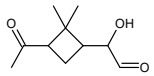	OC(C=O)C1CC(C(C)=O)C1(C)C
Pinic acid / 3-Caric acid	$C_9H_{14}O_4$	186.21	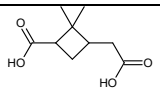	CC1(C(CC1C(=O)O)CC(=O)O)C

Table S1: Instruments operating conditions as described in Gkatzelis et al. (2018).

INSTRUMENT CHARACTERISTICS	ACM (in situ)	CHARON (online)	TD (in situ)
Time resolution (min)	240	1	120
Gas/particle separation	High vacuum	Denuder	Denuder and/or blank correction (filtered air)
Pre-concentration factor	21[a]	44	6000[b]
LOD[c] (ng/m^3)	35[d]	1.4[e]	0.02[b]
Temperature range (°C)	25 – 250	140	25 – 350
Heating rate (°C / min)	100	0	15
Temperature steps (°C)	100, 150, 250 (3 min)	none	None
Desorption pressure (atm)	1	< 1	1
Particle range (nm)	70 – 1000	70 – 1000	70 - 2000
PTR-ToF-MS model	8000	8000	8000
Drift tube Temperature (°C) / Pressure (mbar) / Voltage (V)	90 / 2.3 / 550	120 / 2.4 / 400 and 240	120 / 2.25 / 600
PTR-ToF-MS E/N (Td)	120	65 / 100	160
PTR-ToF-MS mass resolution (m/Δm)	2500	4500-5000	4000

[a] based on 240 min sampling at 80 mL/min and 3 min desorption at 300 mL/min

[b] based on 30 min sampling at 6 L/min and 3 min desorption at 10 mL/min a typical value for most ions based on the method in (Holzinger et al., 2010)

[c] Limit of detection

[d] For signal on *m/z* 139 and 10 sec integration time

[e] For signals around *m/z* 200 and 1 min integration time

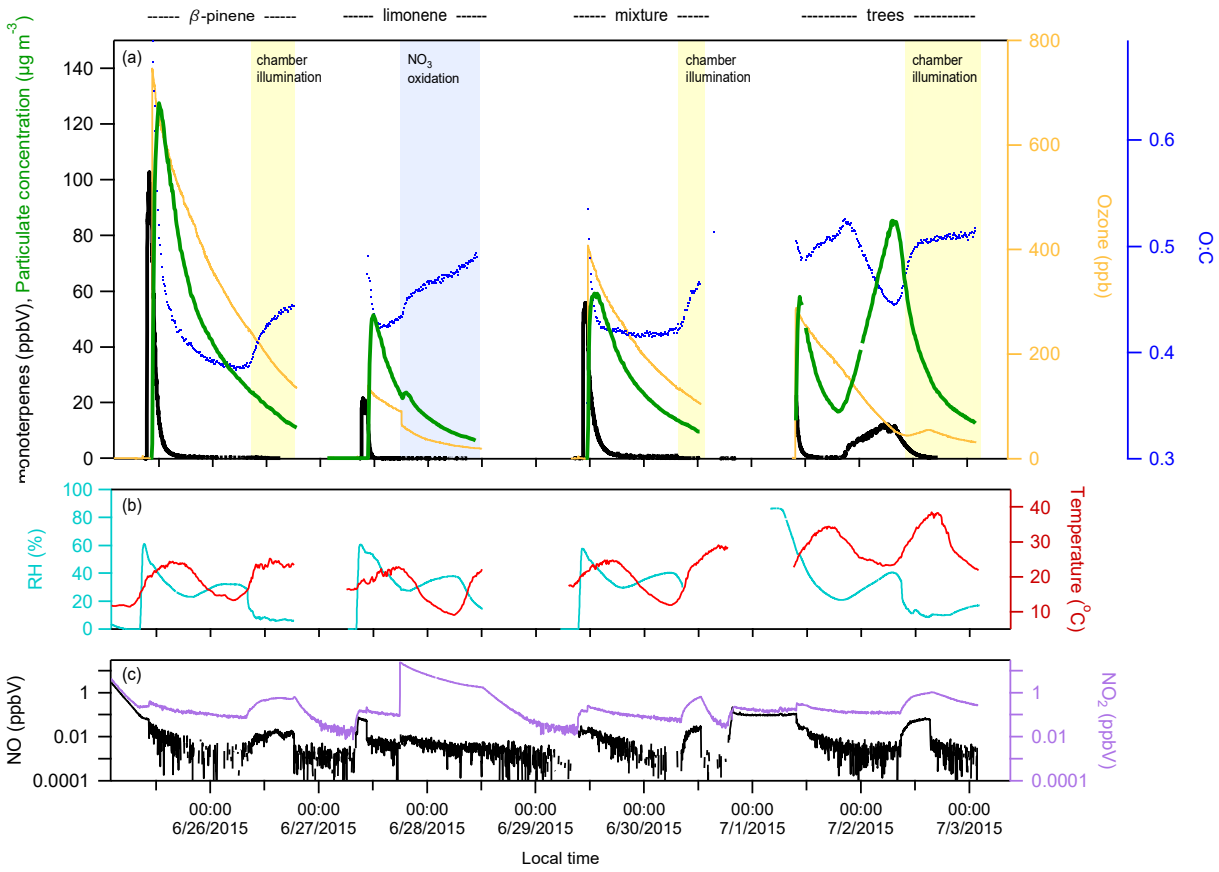

Figure S1: An overview of all experiments during the campaign with (a) corresponding to the mixing ratios of the injected monoterpenes (black line) and ozone (orange line) as well as the SOA mass produced (green line) and its O:C ratio as an indicator of the oxidation of the SOA. Background colours correspond to the opening of the roof (yellow) or the NO_3 oxidation initiation (blue colour). Measurement of the RH (ciel), temperature (red), NO (black) and NO_2 (purple) are also provided.

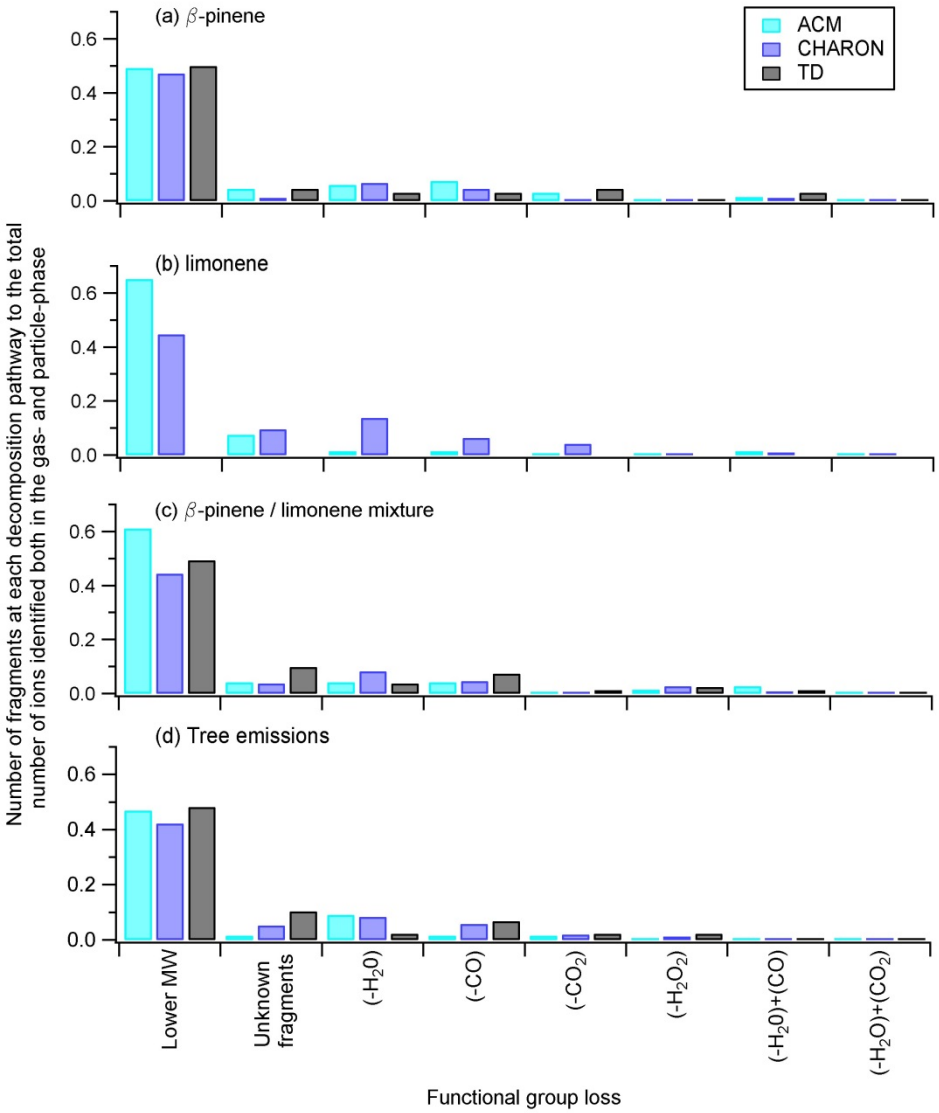

Figure S2: The ratio of the number of lower molecular weight and unknown fragments as well as fragments subject to functional group loss ($(-H_2O)$, $(-CO)$ $(-CO_2)$, $(-H_2O_2)$, $(-H_2O)$ and $(-CO)$, $(-H_2O)$ and $(-CO_2)$) to the number of identified ions both in the gas- and particle-phase. Different colours indicate the different instruments for the different experiments.

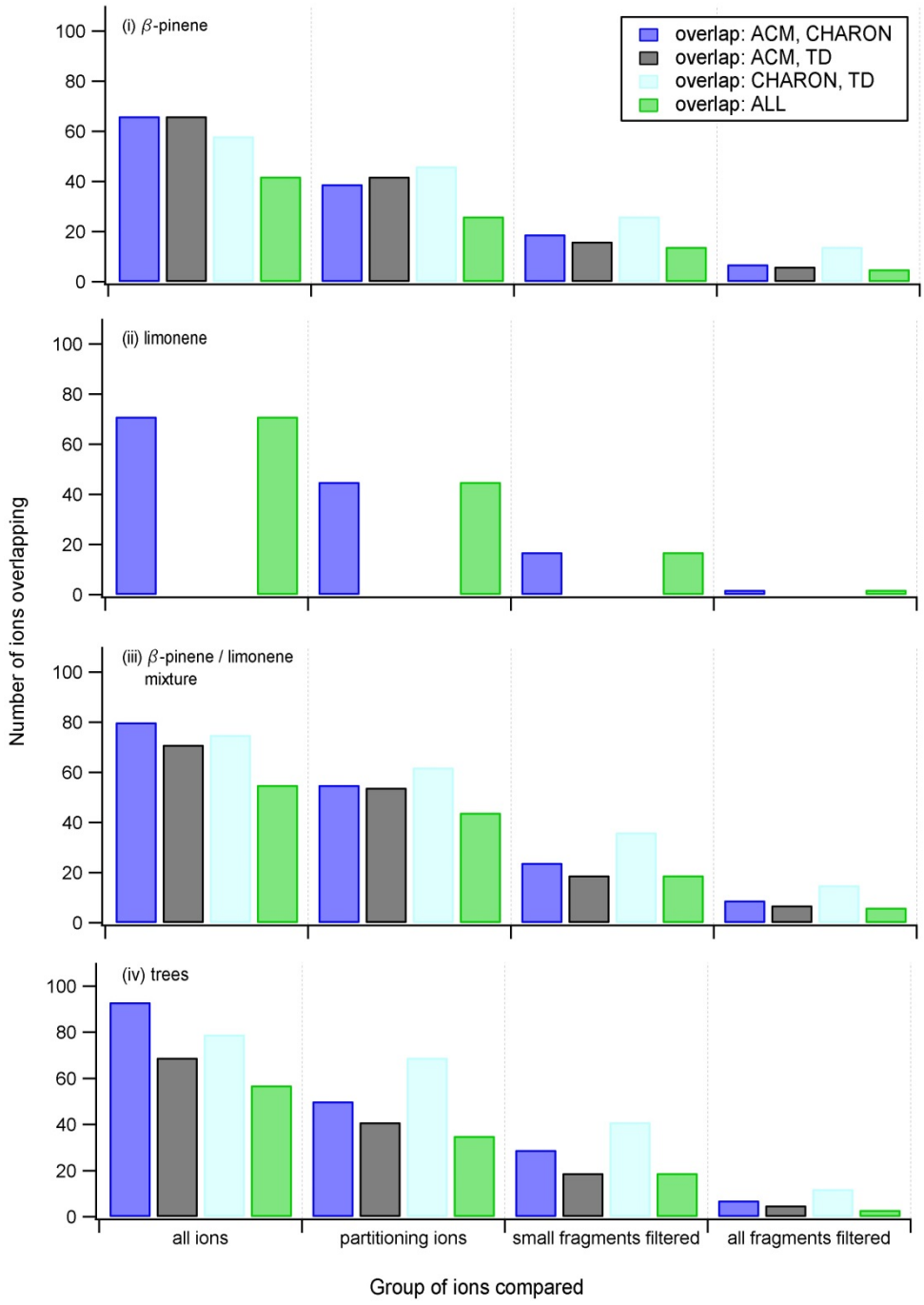

Figure S3: The number of ions measured from more than one technique with a focus on the ions measured both from ACM and CHARON (blue), ACM and TD (black), CHARON and TD (ciel) and ions measured from all techniques, accounting for ACM, TD and CHARON (green). Overlaps are checked for different groups of ions starting from the overlaps of all ions detected, to overlaps seen for only the ions that partition between the gas- and particle-phase, to the overlaps of the remaining partitioning ions after filtering out the small fragments and the remaining partitioning ions after filtering out all fragments for the different experiments performed.

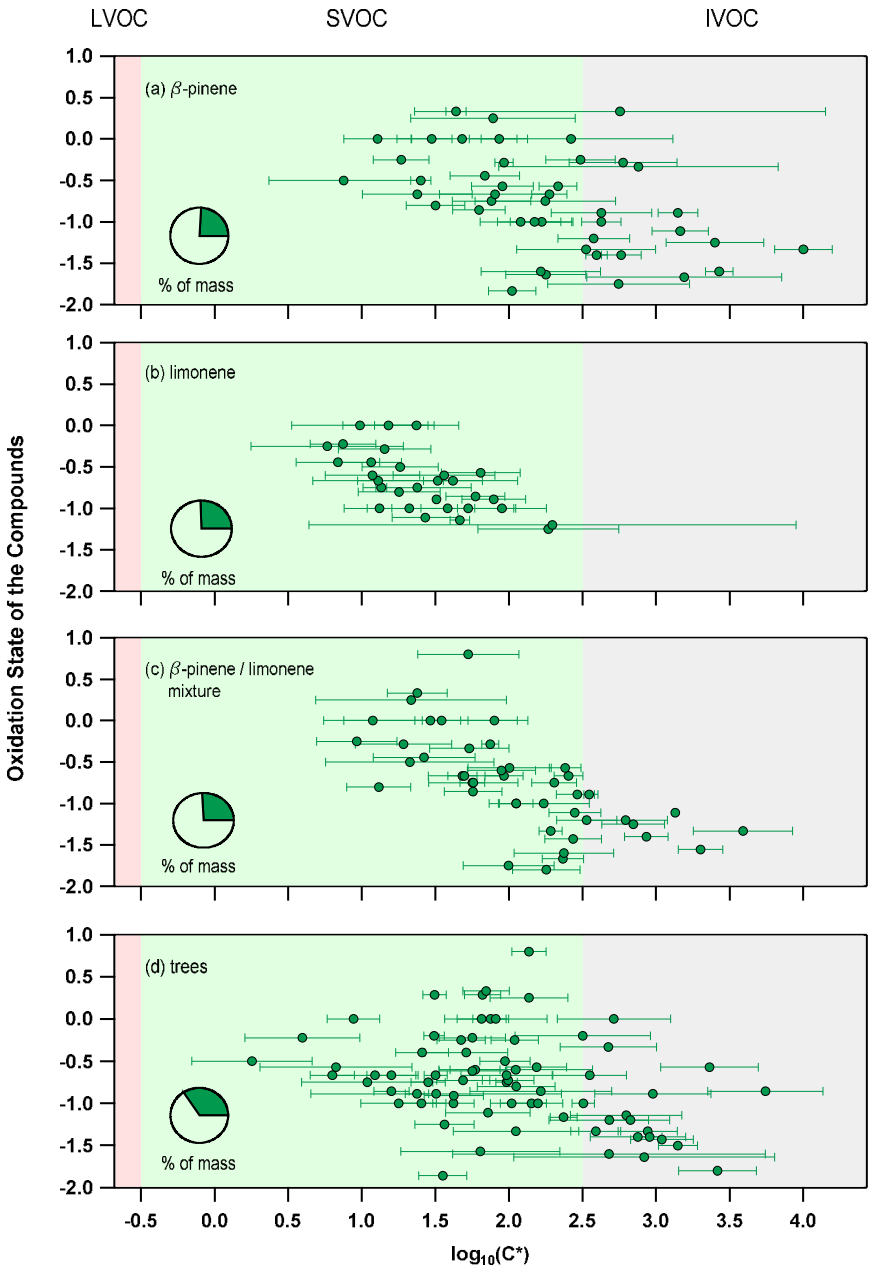

Figure S4: The average experimental saturation concentration for detected ions (from ACM and CHARON) that act as parent ions identified using the described selection criteria during the different experiments. Error bars indicate the ± 1σ of the average. Size of the markers is an indicator of the oxygen atom number for each species. Pie charts show the percent of mass (green) measured when adding all presented ions compared to the total organic mass obtained from the AMS.

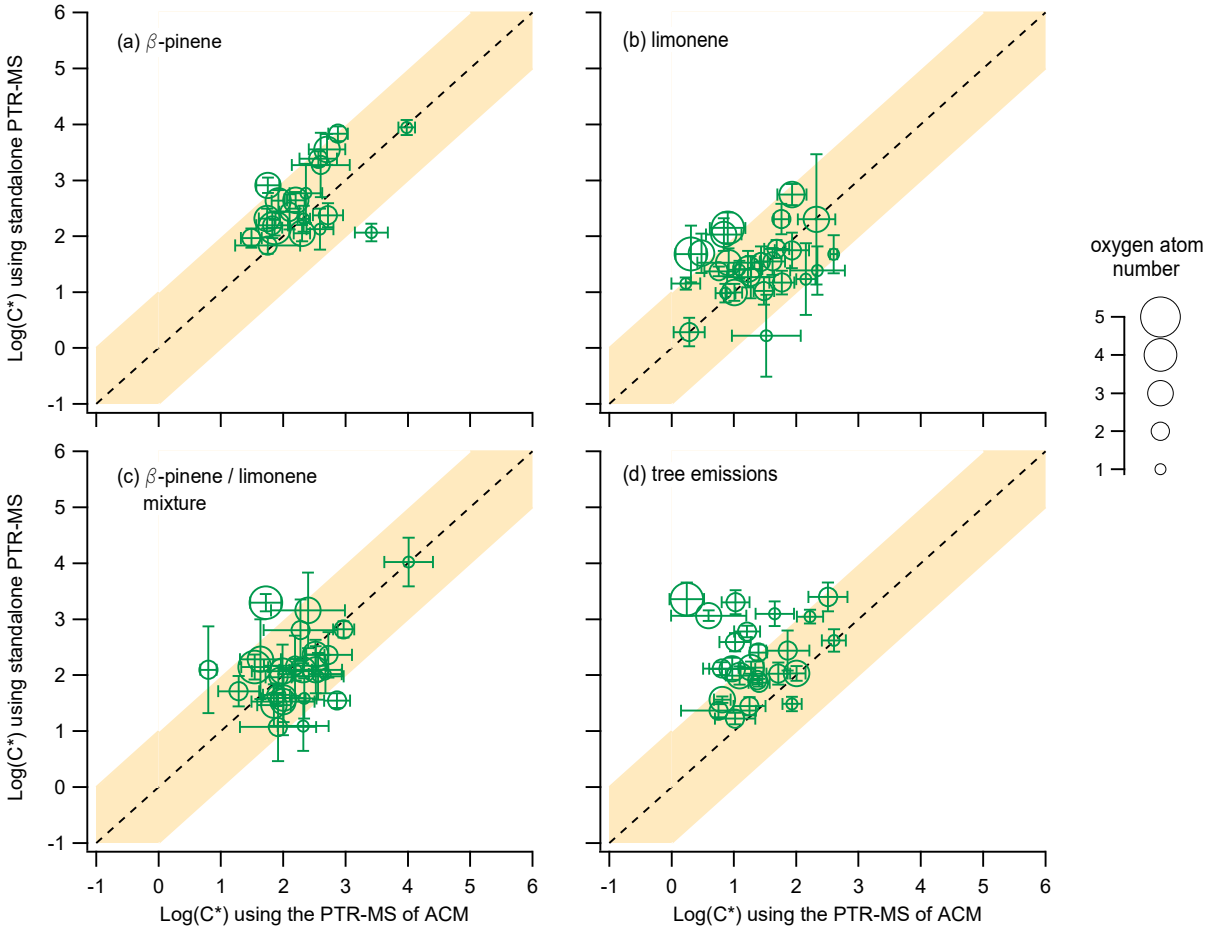

Figure S5: The average saturation mass concentration from the individual experiments for the ACM when using the gas-phase mass concentration values obtained from the PTR-MS of ACM (x-axis) in comparison to the standalone PTR-MS (y-axis). Error bars indicate the ± 1σ of the average. Size of the markers is an indicator of the oxygen atom number for each species.

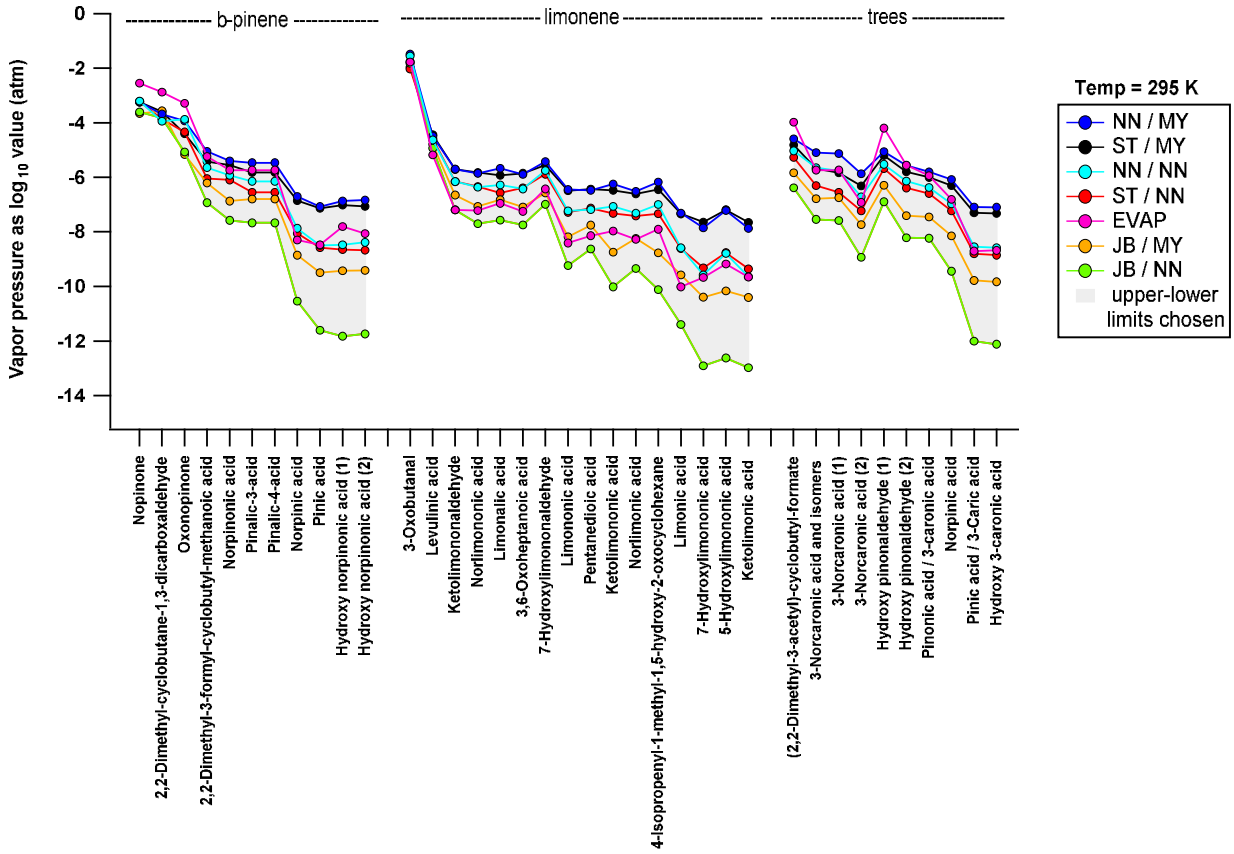

Figure S6: Theoretical calculation of the vapor pressure (y-axis) using the combination of 7 different approaches. The grey background color indicates the minimum and maximum range chosen for this study. Details on the different approaches are provided in section 2.4 and below.

The method originally proposed by Joback and Reid (1987) to predict boiling points based on the molecular structure of the investigated compounds explicitly treats ring increments, which are relevant to monoterpene calculations and thus for this study. Nannoolal et al. (2004) extended the investigated range of functional groups, simultaneously introducing information on a greater neighborhood of the central atom of the investigated functional group. The T_B function fitted to the chosen experimental dataset -enlarged as well - yielded lower boiling points for the compounds investigated here, associated with higher vapor pressure. The method developed by Myrdal and Yalkowsky (1997) includes heat capacity changes for phase transitions into their empirical representation, yielding a lowering in the vapor pressure estimates, compared with the approaches used hitherto (Camredon et al., 2010). The dependency of ΔC_p upon molecular flexibility, i.e. the number of torsional bonds (nonterminal sp^3 and sp^2, rings), makes this inclusion very interesting for monoterpene calculations. Nannoolal et al. (2008) accounted for the heat capacity changes upon vaporization, too. The new feature here is that non-additive interaction contribution of multi-functional groups (e.g OH-ketone) are adopted, resulting in lower vapor pressure values compared with the previous methods. Higher electron delocalization induce stronger dispersive forces, thus decreasing the $p_{i,L}$. This might explain the larger discrepancy between the vapor pressure values calculated by NN/MY and JB/NN with the increasing of alcohol/carbonyl/carboxyl functional group number.

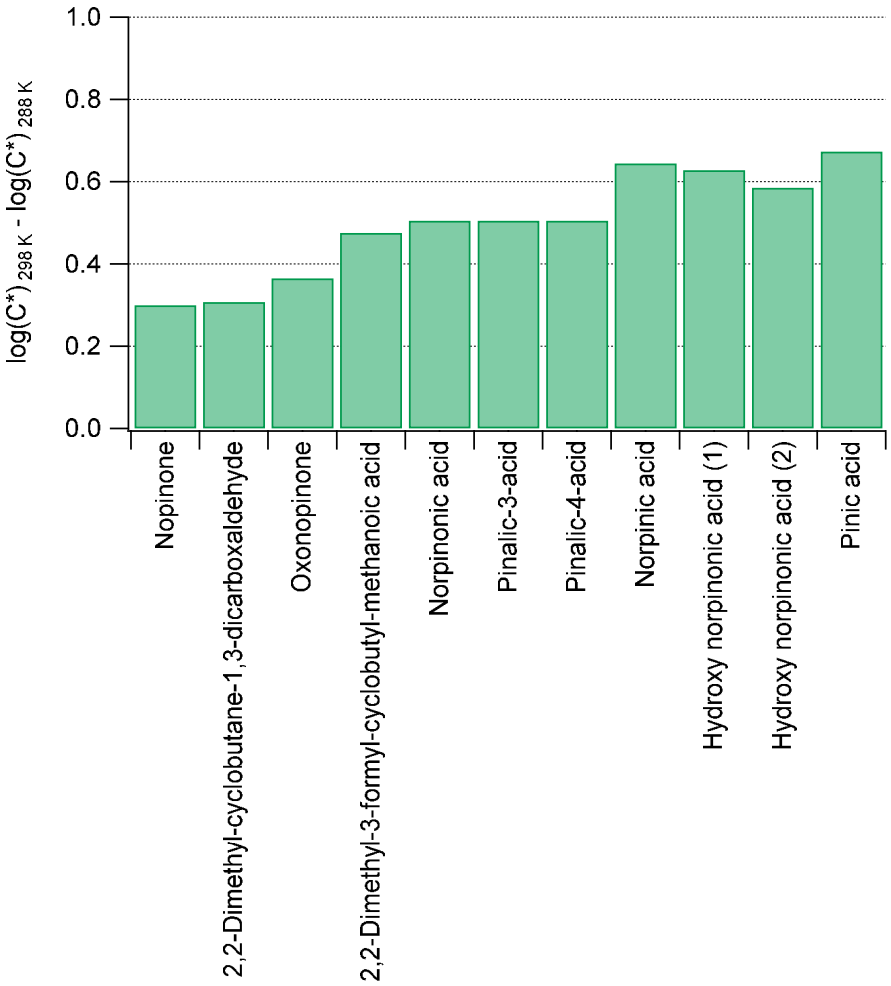

Figure S7: Theoretical calculation of the vapor pressure (y-axis) using the combination of 7 different approaches. To estimate the uncertainty in the experiments due to changes in temperature calculations were also performed at 295 K. Difference in vapor pressure are between 0.3 to 0.6 log(C*).

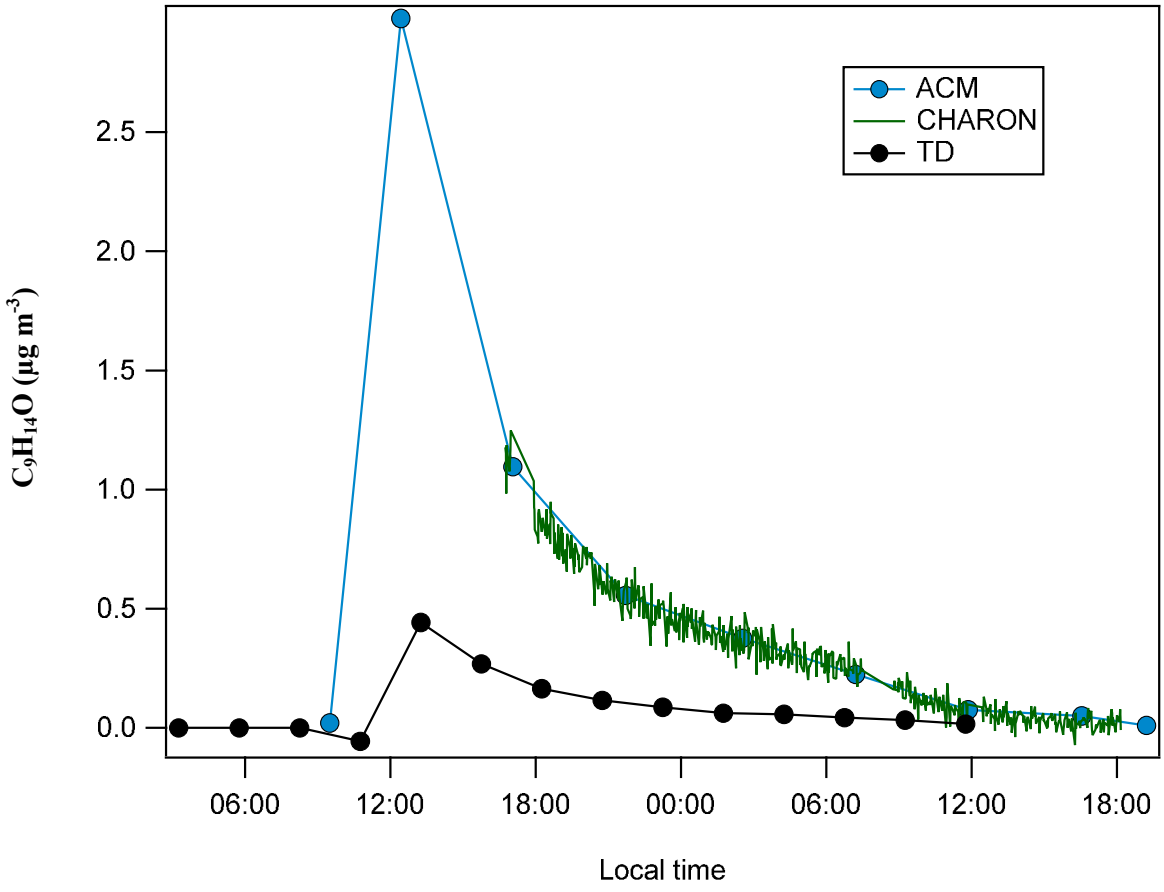

Figure S8: Characteristic example of the timeseries of $C_9H_{14}O$ for the three different inlet techniques

References

Camredon, M., Hamilton, J. F., Alam, M. S., Wyche, K. P., Carr, T., White, I. R., Monks, P. S., Rickard, A. R., and Bloss, W. J.: Distribution of gaseous and particulate organic composition during dark alpha-pinene ozonolysis, Atmos Chem Phys, 10, 2893-2917, DOI 10.5194/acp-10-2893-2010, 2010.

Chen, J., and Griffin, R.: Modeling secondary organic aerosol formation from oxidation of -pinene, -pinene, and -limonene, Atmos Environ, 39, 7731-7744, 10.1016/j.atmosenv.2005.05.049, 2005.

Gkatzelis, G. I., Tillmann, R., Hohaus, T., Müller, M., Eichler, P., Xu, K. M., Schlag, P., Schmitt, S. H., Wegener, R., Kaminski, M., Holzinger, R., Wisthaler, A., and Kiendler-Scharr, A.: Comparison of three aerosol chemical characterization techniques utilizing ptr-tof-ms: A study on freshly formed and aged biogenic soa, Atmos. Meas. Tech., 11, 1481-1500, 10.5194/amt-11-1481-2018, 2018.

Hohaus, T., Gensch, I., Kimmel, J. R., Worsnop, D. R., and Kiendler-Scharr, A.: Experimental determination of the partitioning coefficient of β-pinene oxidation products in soas, Phys Chem Chem Phys, 17, 14796-14804, 10.1039/C5CP01608H, 2015.

Holzinger, R., Kasper-Giebl, A., Staudinger, M., Schauer, G., and Röckmann, T.: Analysis of the chemical composition of organic aerosol at the mt. Sonnblick observatory using a novel high mass resolution thermal-desorption proton-transfer-reaction mass-spectrometer (hr-td-ptr-ms), Atmos Chem Phys, 10, 10111-10128, 10.5194/acp-10-10111-2010, 2010.

Jaoui, M., Corse, E., Kleindienst, T. E., Offenberg, J. H., Lewandowski, M., and Edney, E. O.: Analysis of secondary organic aerosol compounds from the photooxidation of d-limonene in the presence of nox and their detection in ambient pm2.5, Environ Sci Technol, 40, 3819-3828, 10.1021/es052566z, 2006.

Jenkin, M. E.: Modelling the formation and composition of secondary organic aerosol from α- and β-pinene ozonolysis using mcm v3 Atmos Chem Phys, 4, 1741-1757, 2004.

Joback, K. G., and Reid, R. C.: Estimation of pure-component properties from group-contributions, Chemical Engineering Communications, 57, 233-243, 10.1080/00986448708960487, 1987.

Kundu, S., Fisseha, R., Putman, A. L., Rahn, T. A., and Mazzoleni, L. R.: High molecular weight soa formation during limonene ozonolysis: Insights from ultrahigh-resolution ft-icr mass spectrometry characterization, Atmos Chem Phys, 12, 5523-5536, 10.5194/acp-12-5523-2012, 2012.

Leungsakul, S., Jaoui, M., and Kamens, R. M.: Kinetic mechanism for predicting secondary organic aerosol formation from the reaction of d-limonene with ozone, Environ Sci Technol, 39, 9583-9594, 10.1021/es0492687, 2005a.

Leungsakul, S., Jeffries, H. E., and Kamens, R. M.: A kinetic mechanism for predicting secondary aerosol formation from the reactions of d-limonene in the presence of oxides of nitrogen and natural sunlight, Atmos Environ, 39, 7063-7082, 10.1016/j.atmosenv.2005.08.024, 2005b.

Myrdal, P. B., and Yalkowsky, S. H.: Estimating pure component vapor pressures of complex organic molecules, Ind Eng Chem Res, 36, 2494-2499, 10.1021/ie950242l, 1997.

Nannoolal, Y., Rarey, J., Ramjugernath, D., and Cordes, W.: Estimation of pure component properties: Part 1. Estimation of the normal boiling point of non-electrolyte organic compounds via group contributions and group interactions, Fluid Phase Equilibria, 226, 45-63, https://doi.org/10.1016/j.fluid.2004.09.001, 2004.

Nannoolal, Y., Rarey, J., and Ramjugernath, D.: Estimation of pure component properties: Part 3. Estimation of the vapor pressure of non-electrolyte organic compounds via group contributions and group interactions, Fluid Phase Equilibria, 269, 117-133, https://doi.org/10.1016/j.fluid.2008.04.020, 2008.

Praplan, A. P., Schobesberger, S., Bianchi, F., Rissanen, M. P., Ehn, M., Jokinen, T., Junninen, H., Adamov, A., Amorim, A., Dommen, J., Duplissy, J., Hakala, J., Hansel, A., Heinritzi, M., Kangasluoma, J., Kirkby, J., Krapf, M., Kürten, A., Lehtipalo, K., Riccobono, F., Rondo, L., Sarnela, N., Simon, M., Tomé, A., Tröstl, J., Winkler, P. M., Williamson, C., Ye, P., Curtius, J., Baltensperger, U., Donahue, N. M., Kulmala, M., and Worsnop, D.

R.: Elemental composition and clustering of α-pinene oxidation products for different oxidation conditions, Atmos Chem Phys Disc, 14, 30799-30833, 10.5194/acpd-14-30799-2014, 2014.

Yu, J., Cocker, D. R., Griffin, R. J., Flagan, R. C., and Seinfeld, J. H.: Gas-phase ozone oxidation of monoterpenes: Gaseous and particulate products, J Atmos Chem, 34, 207-258, 10.1023/a:1006254930583, 1999.